GEOPHYSICAL RESEARCH LETTERS, VOL. 32, L22304, doi:10.1029/2005GL024026, 2005

Waveform inversion of the S reflector west of Spain: Fine structure of a detachment fault

T. Leythaeuser and T. J. Reston
IFM-GEOMAR, Leibniz-Institute of Marine Sciences, Kiel, Germany

T. A. Minshull
National Oceanography Centre, Southampton, UK

Received 8 July 2005; revised 22 September 2005; accepted 4 October 2005; published 17 November 2005.

[1] The S reflection west of Iberia has been interpreted as a low-angle detachment fault separating crustal fault blocks from partially serpentinized mantle. We apply full waveform inversion to investigate the fine structure of S. Our results confirm that S is largely a step increase in velocity (and density), probably from crustal rocks to partially serpentinized mantle peridotites. A ~50 m thick low velocity zone above S might represent a main fault zone of highly serpentinized peridotites or hydrofractured and altered crustal rocks above the main fault zone. Both interpretations imply focused fluid flow along S, raising the possibility that low-angle movement along S was aided by the development of local, transient high fluid pressures. **Citation:** Leythaeuser, T., T. J. Reston, and T. A. Minshull (2005), Waveform inversion of the S reflector west of Spain: Fine structure of a detachment fault, *Geophys. Res. Lett.*, *32*, L22304, doi:10.1029/2005GL024026.

1. Introduction

[2] The breakup of non-volcanic continental margins appears in several cases to be associated with the development of detachment faults and the unroofing of mantle peridotites [e.g., *Pérez-Gussinyé and Reston*, 2001]. The classic example of this pattern is the deep west Galicia rifted margin (Figure 1), where the S-reflector is generally interpreted as a detachment fault, separating continental fault blocks from underlying partially serpentinized mantle [*Reston et al.*, 1996] which crops out farther west at the ''Peridotite Ridge'' [*Boillot et al.*, 1995]. Although the footwall to S has not been sampled, the footwall to the similar H-reflector has been drilled and serpentinized peridotites recovered [*Whitmarsh et al.*, 2001], increasing confidence that such serpentinites are also present beneath S. Furthermore, wide-angle data [*Zelt et al.*, 2003] indicate that below S velocity increases from ~7 km/s to 7.6 km/s, consistent with downward decreasing amounts of serpentinization.

[3] S is identified as a detachment fault as on depth sections (Figure 1) it passes undisturbed beneath the tilted fault blocks; the block-bounding faults stop abruptly at S [*Reston et al.*, 1996]. The physical cause of the reflection from S has been interpreted on the basis of waveform and attribute analysis as being a step in seismic velocity and density [*Reston*, 1996], implying that the detachment fault is a sharp tectonic boundary between two very different rock types. However several key questions remain. For instance, although S appears related to mantle serpentinization, it is unclear what is the relationship between serpentinization and deformation in the vicinity of the fault. Furthermore, *Reston* [1996] noted that even if S is a step increase in acoustic impedance, this might indicate a zone above S in which velocity decreases gradually downwards due to brecciation and increasing water content as much as the presence of high velocity rocks beneath S. Finally, seismic images [*Reston et al.*, 1996] (Figure 1) suggest that S was active at ~10°, lower than permitted just by the presence of weak fault gouge [*Wills and Buck*, 1997; *Abers*, 2001], raising the possibility that movement was facilitated by high fluid pressures. In this paper we use waveform inversion to investigate the details of the transition across the S-reflector.

0094-8276/05/2005GL024026$05.00

2. Data and Pre-Processing

[4] The data used in the paper comes from the Iberia Seismic Experiment (ISE) cruise with the RV Maurice Ewing [*Zelt et al.*, 2003], and were collected with a 160 channel 4 km streamer, and a large tuned seismic array. The data were split into several processing schemes: one set underwent waveform deconvolution to remove residual bubble effects, amplitude balance, and prestack depth migration, resulting in both an optimum depth image and a detailed velocity model above the S reflector through depth-focussing error analysis [e.g., *Reston et al.*, 1996] and Common Reflection Point (CRP) gather analysis. The other data stream went into the full waveform inversion procedure.

3. Full Waveform Inversion

[5] The full waveform inversion applied aims to find a seismic model of the subsurface that minimizes misfit between real and synthetic data. Minimization of misfit is based on the conjugate optimization scheme [*Kormendi and Dietrich*, 1991]; the subsurface reflectivity is calculated using the generalized reflection and transmission matrix of *Kennett and Kerry* [1979], accurately treating multiples, mode conversions and other nonlinear effects. The reflectivity is then convolved with the wavelet to generate synthetic traces. This technique has been used to determine the fine structure of other key reflectors, such as gas hydrate reflectors [*Minshull et al.*, 1994], and of the melt lens at a fast-spreading mid-ocean ridge [*Collier and Singh*, 1997].

[6] The source waveform (Figure 2) and seabed reflectivity were extracted from the data through a comparison

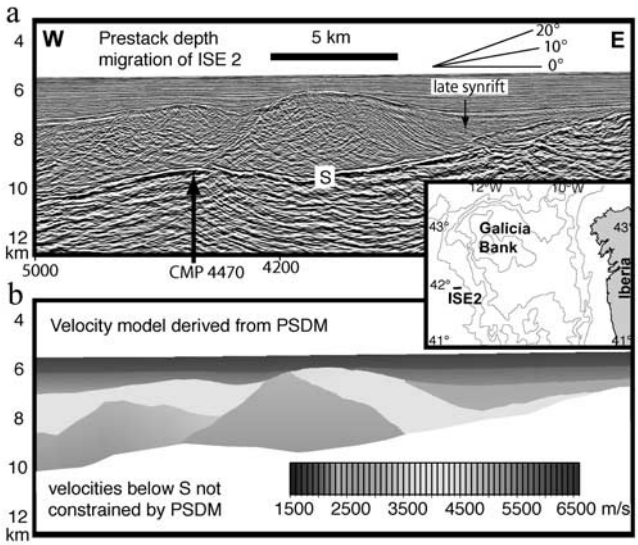

Figure 1. A: Image of S derived by iterative prestack depth migration (PSDM) of profile ISE2, showing location chosen for waveform inversion. S is here sub-horizontal; S generally dips < 10° to the west. B; detailed velocity model derived iteratively by PSDM and depth-focussing error/CRP gather analyses, providing background velocity above S for the inversion. Inset map shows profile location.

between the seafloor reflection and its multiple [*Minshull et al.*, 1994; *Warner*, 1990]. Ideally this should be carried out in the same location as the inversion, but there the multiple is below the data window, so we extracted the source waveform slightly further up the slope. Observers logs noted no change in the shooting configuration between the two locations. The seafloor reflection coefficient of 0.22 at near-normal incidence agrees with previous results [*Reston*, 1996] and was used to constrain the velocity-depth function of the seafloor in the starting model. The source is assumed to be isotropic for the frequencies and slownesses used in the inversion; estimated source and receiver directivity effects are less than 10% for the maximum slowness used at the depth of the S reflector.

[7] The initial velocity model above S (Figure 2) was derived from pre-stack depth migration (Figure 1) using a combination of densely sampled common-reflection point analysis and depth-focussing error analysis [*Reston et al.*, 1996]. As there are no coherent reflections beneath S, velocities below S were derived from OBS and OBH data [*Zelt et al.*, 2003] which show that S is marked by an increase to velocities of 7.0 km/s increasing downwards over the next 1-2 km to 7.6 km/s (probably reflecting downward decreasing amounts of serpentinization). The velocity model was sampled at 10 m intervals and then averaged over a 26 m sliding window to remove major velocity steps. The initial Vs and density models were derived from this Vp model (Figure 2) using standard relationships [*Ludwig et al.*, 1970]. Although such relationships do not explicitly include serpentinites, at the velocity range in question serpentinites have similar physical properties to gabbros [*Horen et al.*, 1996]. Q values (Qp in sediments of 200 and in crust of 400; Qs in sediments of 25 and in crust of 100) were chosen to be consistent with previous estimates of Q [e.g., *Boillot et al.*, 1995; *Reston*, 1996] from the area.

[8] The inversion is applied to a common-midpoint (CMP) gather and assumes that the structure is laterally continuous, i.e. one-dimensional. Because the inversion is 1D, it is not suitable where structure is complex or target reflections variable, discontinuous or incoherent. As a result, we selected a portion of the data where both S and the overlying structure were as flat and as far as possible from interfering reflections. Over 500 m. to the east, a weak reflection from a block-bounding fault intersects and distorts S, but does not affect the waveform at our chosen location. Although, complex trace analysis [*Reston*, 1996] shows that the waveform of S is stable over several km both in the dip and strike direction, final proof of the validity of the 1D assumption will require 3D data. This should be borne in mind when considering the significance of the results.

[9] The inversion is carried out in the frequency-slowness domain (ω-p): to ensure correct transformation without spatial aliasing, we first generated a super CMP gather by merging four adjacent CMP gathers (4470–4473) containing the complete range of offsets. The waveform inversion is carried out as a series of five runs, each containing 15 iterations, with increasing ranges of frequency and slowness. This approach contrasts with gradient-based inversions (which converge to a local minimum of the misfit function) by accounting for longer wavelength changes in the velocity-depth function before determining the finer details of the velocity structure. The final model of each run was used as the starting model for the first iteration of the next run.

[10] The last few iterations of the fifth run resulted in very little change of the misfit function (0.45%), indicating convergence to a minimum value. Only the p-wave velocity was inverted, so that the inversion is strictly only for Vp, keeping Vs and density constant during all the runs. As a result, the absolute values of the fine structure revealed by the inversion are unlikely to be accurate and more an indication of the variations in acoustic impedance than in Vp.

4. Results

[11] The quality of the inversion can be seen by the close match between the real and synthetic S reflection (Figure 3).

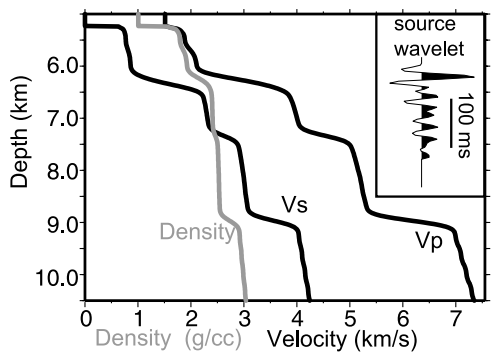

Figure 2. Initial velocity-density model and source wavelet. Vs: shear wave velocity; Vp: p-wave velocity.

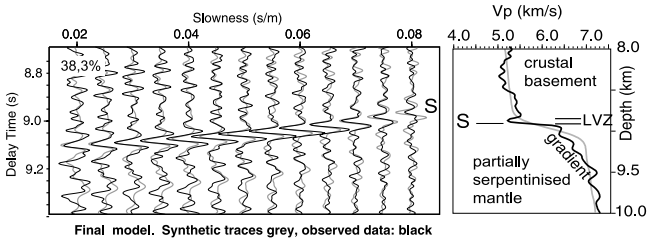

Figure 3. Comparison of synthetic results with original traces around S. The match is very good for S – a misfit of 38.3% in a 350 ms window about S results. Right: Final velocity model (black) overlain on initial Vp model (gray), showing fine structure revealed by the inversion. Note the presence of a 50 m. low velocity zone (LVZ) immediately above S and a gradient zone below S. S itself is resolved as a sharp step increase in velocity, not present in the starting model.

The misfit is greatest for both the lowest and highest values of slowness, corresponding to the nearest and furthest offsets. The former may be explained by the increased noise levels on the near offsets; the latter by the increasing deviation from the 1-D velocity assumption at the far offsets, particularly as raypaths approach the fault block edge.

[12] The final velocity model (Figure 3) shows fine structure over intervals too small to be resolved by PSDM or wide-angle modeling. For instance, beneath the S reflector, the velocity is almost 500 m/s less than determined from the wide-angle data, but increases over 500 m to close to the wide-angle value. We believe that this discrepancy reflects the limited resolution of the wide-angle tomographic inversion (node spacing of 750 m) [*Zelt et al.*, 2003]. The fine velocity structure may indicate a broad zone of increasing velocity/decreasing degree of serpentinization moving down from the fault.

[13] Immediately above S, the waveform inversion indicates a narrow zone of reduced velocity (Figure 3), corresponding to a local decrease in near-vertical p-wave acoustic impedance of about 5%. Even with optimum thin layer tuning, the negative reflection coefficient above S contributes less than one fifth of the overall amplitude of the S reflection – the amplitude of the S reflection is dominated by the underlying increase in velocity and density, consistent with the previous conclusions [*Reston*, 1996].

[14] We investigated how well the inversion constrains the thickness of the LVZ by replacing that produced by the inversion with a sharp low velocity layer of similar thickness (50 m) and one 100 m thick (Figure 4). The fit with the 50 m LVZ is statistically even better than the final velocity model, but the 100 m LVZ produces a noticeably poorer fit both statistically and visually. We thus conclude that the thickness of the LVZ of 50m is reasonably well constrained.

[15] We investigated other starting models with various Q functions and different velocity (and density) functions in the vicinity of S. These either yielded similar results (S as a step increase in acoustic impedance overlain by a low velocity zone) or produced an unacceptable mismatch between observed and synthetic data. For instance, after 5 runs (each of 15 iterations) with a starting model (Figure 5) with no strong discontinuity at S (thus requiring a higher velocity above S to match the wide-angle results), the inversion produced a velocity model consisting of a step increase at S, overlain and underlain by LVZs. However, the match in terms of both waveform and amplitude is noticeably poor at S, and the intercept time is poorly reproduced at low and high slowness – an indication that the velocity above S is wrong. The failure of this run suggests that the velocity resolution of the reflection data is rather good (better than 200 m/s for the block above S), and that S must represent a substantial step increase in velocity to explain its amplitude and waveform.

5. Discussion

[16] In common with most studies of rifted margins, we assume that the main features of basement structure developed during rifting and that the undisturbed postrift sequence prevented further substantial water-rock interaction. In particular we consider that the large volumes of fluids needed to serpentinize the mantle and to produce a low-velocity fault zone can only reach the subsurface during active faulting [*Pérez-Gussinyé and Reston*, 2001].

[17] While bearing in mind the limitations of a 1D inversion, the results appear to provide two lines of evi-

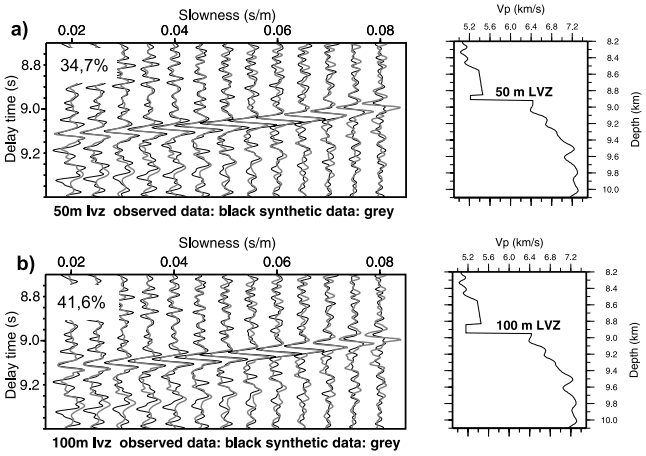

Figure 4. Comparison between real data and synthetics based on simplified structure of LVZ above S. When the LVZ is a sharp 50 m thick layer (top), the calculated misfit (34.7%) is slightly lower than for the preferred final model (Figure 3). For a 100 m. thick LVZ (below), the fit is visually and statistically poorer.

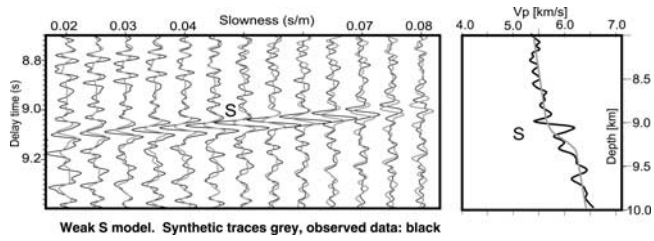

Figure 5. Inversion resulting from alternative starting model (gray line on right), with little velocity increase at S. The inversion develops a velocity step at S with pronounced LVZ both above and below as it tries to keep to the initial gradient. The fit at S is poor in terms of amplitude, waveform and (at high slowness) delay time.

dence for (syntectonic) fluid concentration along S. First, the section immediately beneath S is marked by a strong acoustic impedance gradient, interpreted as downward decreasing degrees of serpentinization and hence fluid availability. Second, the section immediately above S is marked by a local decrease in acoustic impedance. We suggest that this low velocity zone may also reflect fluid concentration during rifting. In one interpretation, this "low velocity zone" (LVZ) might correspond to (~80%) hydrated/serpentinized peridotites along the fault. (Fault rocks recovered from a ~30° fault from the Woodlark Basin included chlorite and talc schists) [*Floyd et al.*, 2001]. In this case, the lithological crust-mantle boundary and main tectonic contact would occur at the top of the LVZ, and the base of the LVZ would correspond to a transition to less serpentinized rocks with increasing depth. However, the upper boundary of the LVZ appears more transitional than the lower one.

[18] Alternatively, the gradual decrease in velocity moving up to S may reflect increasing serpentinization and the main velocity jump at S a sudden *lithological* change to the overlying crustal fault blocks, with the region of reduced velocity immediately above the main S detachment. Such a zone of reduced velocity may indicate a zone of hydrofracturing of the base of the crustal fault blocks and is consistent with the highly brecciated units present above some detachment faults in the western US [*Reston*, 1996].

[19] In either case, we suggest that fluids were probably concentrated along S during extension and mantle unroofing. If hydrofracturing occurred it is also likely that the fluid was at least transiently overpressured. Even a slight degree of overpressure, coupled with the presence of weak mantle serpentinites along the fault would allow the S detachment to have been active at low angles [*Reston et al.*, 1996]. Although permanently high fluid pressures would contradict the traditional view that little overpressure can develop in an extensional system [e.g., *Scholz*, 1992; *Wills and Buck*, 1997], *Wills and Buck* [1997] accept that "evidence for locally high pore pressures in normal fault zones is, indeed, compelling". We suggest that such pressures developed transiently and locally along S due to the volume increase associated with serpentinization: as water passes through part of a fault network, it reacts with the peridotitic wall-rock to produce serpentine. The resulting volume expansion acts both to seal parts of the fault, and to push on the other sealed compartments of the fault or on other fault strands. Once a segment of the fault is sealed, it is hydrologically isolated from the surface and internal pressures can increase towards lithostatic. Fluid pressure in the sealed segments is only relieved when the fault ruptures: the development of numerous small sealed pockets segments along the fault may favor rupture along the length of the fault, i.e. low-angle slip.

[20] **Acknowledgments.** This work was supported by the DFG under grant Re 873/6 and by the EU through the Marie Curie program (contract HPMT-CT-2000-00122). Processing of the reflection data was carried out with the Sirius ® software of GX technology and using the Seismos ® software of Western Geco-Prakla. We thank Dirk Klaeschen for help with data processing. The data were collected in collaboration with Rice University, cruise leader Dale Sawyer. We thank the captain and crew of the RV Ewing for their professionalism and dedication.

References

Abers, G. A. (2001), Evidence for seismogenic normal faults at shallow dip in continental rifts, *Spec. Publ. Geol. Soc. London*, *187*, 305–318.

Boillot, G., M.-O. Beslier, C. M. Krawczyk, D. Rappin, and T. J. Reston (1995), The formation of a passive margin: Constraints from crustal structure and segmentation of deep Galicia margin, *Spec. Publ. Geol. Soc. London*, *90*, 71–92.

Collier, J. S., and S. C. Singh (1997), Detailed structure of the top of the melt body beneath the East Pacific Rise at 9 degrees 40′N from waveform inversion of seismic reflection data, *J. Geophys. Res.*, *102*, 20,287–20,304.

Floyd, J. S., J. C. Mutter, A. M. Goodliffe, and B. Taylor (2001), Evidence for fault weakness and fluid flow within an active low-angle normal fault, *Nature*, *411*, 779–783.

Horen, H., M. Zamora, and G. Dubuisson (1996), Seismic waves velocities and anisotropy in serpentinized peridotites from Xigaze Ophiolite: Abundance of serpentine in slow spreading ridge, *Geophys. Res. Lett.*, *23*, 9–12.

Kennett, B. L. N., and N. J. Kerry (1979), Seismic waves in a stratified halfspace, *Geophys. J. R. Astron. Soc.*, *57*, 557–583.

Kormendi, F., and M. Dietrich (1991), Nonlinear waveform inversion of plane-wave seismograms in stratified elastic media, *Geophysics*, *56*, 664–674.

Ludwig, W. J., J. E. Nafe, and C. L. Drake (1970), Seismic refraction, in *The Sea*, vol. 4, part 1, edited by A. E. Maxwell, pp. 53–84, Wiley-Interscience, Hoboken, N. J.

Minshull, T., S. Singh, and G. K. Westbrook (1994), Seismic velocity structure at a gas hydrate reflector, offshore western Colombia from full waveform inversion, *J. Geophys. Res.*, *99*, 4715–4734.

Pérez-Gussinyé, M., and T. J. Reston (2001), Rheological evolution during extension at passive non-volcanic margins: Onset of serpentinization and development of detachments to continental break-up, *J. Geophys. Res.*, *106*, 3691–3975.

Reston, T. J. (1996a), The S reflector west of Galicia: The seismic signature of a detachment fault, *Geophys. J. Int.*, *127*, 230–244.

Reston, T. J., C. M. Krawczyk, and D. Klaeschen (1996b), The S reflector west of Galicia: Evidence from prestack depth migration for detachment faulting during continental breakup, *J. Geophys. Res.*, *101*, 8075–8091.

Scholz, C. H. (1992), Weakness amidst strength, *Nature*, *349*, 677–678.

Warner, M. (1990), Absolute reflection from deep seismic reflections, *Tectonophysics*, *173*, 15–23.

Whitmarsh, R. B., G. Manatschal, and T. A. Minshull (2001), Evolution of magma-poor continental margins from rifting to seafloor spreading, *Nature*, *413*, 150–154.

Wills, S., and W. R. Buck (1997), Stress field rotation and rooted detachment faults: A Coulomb failure analysis, *J. Geophys Res.*, *102*, 20,503–20,514.

Zelt, C. A., K. Sain, J. V. Naumenko, and D. Sawyer (2003), Assessment of crustal velocity models using seismic refraction and reflection tomography, *Geophys. J. Int.*, *153*, 609–626.

T. Leythaeuser and T. J. Reston, IFM-GEOMAR, Leibniz-Institute of Marine Sciences, D-20148 Kiel, Germany. (treston@ifm-geomar.de)

T. A. Minshull, National Oceanography Centre, Southampton SO14 3ZH, UK.